Tellus (1989), *41A*, 338–356

Retrieval of microphysical variables by a diagnostic modelling study: comparison between parameterized and detailed warm microphysics

By M.-N. LE CAM and H. ISAKA, *LAMP/OPGC, UA CNRS no. 267, Université Blaise Pascal (Clermont-Ferrand II), B.P. 45, 63170-Aubiere, France*

(Manuscript received 27 April 1987; in final form 10 September 1988)

ABSTRACT

Retrieval of microphysical fields associated with a wind field deduced from Doppler radar data is performed with a model based on the use of continuity equations for heat and water substance. Both detailed and parameterized microphysical schemes have successively been incorporated in the model and fields retrieved from both schemes are compared in the case of the convective part of a tropical squall line. The retrieved fields display fairly similar features when considered for the whole convective region. However, the efficiency of microphysical processes responsible for the production of rain at local scale depends on the microphysical scheme incorporated in the model. The rate of evaporation of rain in unsaturated air is also sensitive to the microphysical scheme. Both models are able to reproduce intense precipitation observed by the radars and a rain gauge with a slightly better agreement in the case of the detailed model. Drop size distributions simulated by the detailed model are analyzed in relation to their normalization, effective precipitation processes and wind field. In zones of intense precipitation, they display features similar to those of a gamma distribution. In convective zones with intense updraughts, they display quite different features. Implications for the interpretation of integrated parameters of size distributions of rain are examined.

1. Introduction

During past decades, theoretical and laboratory studies have led to a better understanding of some basic microphysical processes. Nonetheless, the development of precipitation in a real cloud is still poorly understood, since the effective formation of precipitation is the result of complex interactions between these basic processes, highly conditioned by dynamic and thermodynamic characteristics of the cloud; its study has been hampered by a limited knowledge of these cloud characteristics, due to the difficulty of measurement.

In order to remedy this lack of observations, some attempts have recently been made to retrieve microphysical and thermal fields from Doppler radar observations. The method of retrieval is based on the combination of a numerical kinematic cloud model with experimental wind fields derived from Doppler radar data (Rutledge and Hobbs, 1983, 1984; Ziegler, 1985; Hauser and Amayenc, 1986). Such thermal and microphysical fields are internally consistent with observed airflow in the cloud. Their analysis may provide useful information about the effective precipitation mechanisms in relation to the wind field. However, the realism of the retrieved thermal and microphysical fields necessarily depends on the characteristics of the model on which the retrieval is based, especially on its microphysical scheme. The performance of the method should, therefore, be evaluated by comparing the retrieved microphysical fields with the observed ones (radar reflectivity, precipitation rate, nature and size distribution of microphysical constituents observed in situ by instrumented aircraft ...). The purpose of the present study is to examine the sensitivity of this type of retrieval method to the choice of the microphysical scheme. The cloud model developed in this paper is analogous to those of Rutledge and Hobbs (1984) and Ziegler (1985). Two versions of the model have been implemented; the first one, called model with detailed microphysics (MDM for short), uses a discrete set of size categories to represent condensed water and describes the microphysical processes in detail, and the second one, called model with parameterized microphysics (MPM for short), uses the parameterization of Kessler (1969). The description of the model is given in Section 2. The performance of both versions is then evaluated in the simulation of precipitation formation within the convective part of a tropical squall line observed on 22 June 1981, during the COPT 81 experiment. Differences between microphysical fields and water budget deduced from both versions of the model are discussed with respect to efficiencies of microphysical processes. Finally, drop size distributions simulated by the model with detailed microphysics are analysed and some implications for the use of integrated parameters of size distributions are deduced.

2. The model

In this method of retrieval, a system of continuity equations for heat, water vapour and condensed water is solved for a fixed wind field and initial fields of temperature and humidity. The integration of the equations is performed forward in time until steady fields of temperature and water substance are reached. Both versions (MDM and MPM) are presently limited to warm microphysics in a two-dimensional framework.

The temperature T and the water vapour mixing ratio q_v are prognostic variables common to both models, while prognostic variables describing condensed water differ according to the incorporated microphysical scheme. In the MDM case, condensed water, distributed into a discrete set of N size categories, is represented by the number concentration of drops n_i per unit volume in the ith size category (a drop belonging to the ith size category is noted an "i-drop" in the present paper). Activated cloud condensation nuclei are also represented by their number concentration n_{ac}. In the MPM case, condensed water is divided into two categories: cloud water which shares the airflow and rain water which precipitates. Both are represented by their mixing ratios, denoted q_c and q_r respectively.

2.1. Continuity equations

The equations for the temperature T and the water vapour mixing ratio q_v are common to both models. They are given by:

$$\frac{\partial T}{\partial t} = -u\frac{\partial T}{\partial x} - w\frac{\partial T}{\partial z} - w\Gamma_d + \left(\frac{\partial T}{\partial t}\right)_{CE}, \tag{1}$$

$$\frac{\partial q_v}{\partial t} = -u\frac{\partial q_v}{\partial x} - w\frac{\partial q_v}{\partial z} + \left(\frac{\partial q_v}{\partial t}\right)_{CE}. \tag{2}$$

In these equations, u and w denote, respectively, the horizontal and vertical wind components deduced from Doppler radar data and Γ_d the dry adiabatic lapse rate. In each equation, the first two terms represent advection with the airflow, and the last term represents the effect of the condensation/evaporation process.

The microphysical equations are given in the MDM case by:

$$\begin{aligned}\frac{\partial n_i}{\partial t} &= -u\frac{\partial n_i}{\partial x} - w\frac{\partial n_i}{\partial z} + \frac{n_i w}{\rho_a}\frac{\partial \rho_a}{\partial z} + \delta_i\left(\frac{\partial n_i}{\partial t}\right)_{ACT} \\ &+ \left(\frac{\partial n_i}{\partial t}\right)_{CE} + \left(\frac{\partial n_i}{\partial t}\right)_{CC} + \left(\frac{\partial n_i}{\partial t}\right)_{CB} + \left(\frac{\partial n_i}{\partial t}\right)_{SB} \\ &+ \left(\frac{\partial n_i}{\partial t}\right)_{SED}, \quad i = 1, \dots N,\end{aligned} \tag{3}$$

$$\frac{\partial n_{ac}}{\partial t} = -u\frac{\partial n_{ac}}{\partial x} - w\frac{\partial n_{ac}}{\partial z} + \frac{n_{ac} w}{\rho_a}\frac{\partial \rho_a}{\partial z} + \left(\frac{\partial n_{ac}}{\partial t}\right)_{ACT}, \tag{4}$$

and in the MPM case by:

$$\begin{aligned}\frac{\partial q_c}{\partial t} &= -u\frac{\partial q_c}{\partial x} - w\frac{\partial q_c}{\partial z} + \left(\frac{\partial q_c}{\partial t}\right)_{CE} + \left(\frac{\partial q_c}{\partial t}\right)_{AUT} \\ &+ \left(\frac{\partial q_c}{\partial t}\right)_{ACC},\end{aligned} \tag{5}$$

$$\begin{aligned}\frac{\partial q_r}{\partial t} &= -u\frac{\partial q_r}{\partial x} - w\frac{\partial q_r}{\partial z} + \left(\frac{\partial q_r}{\partial t}\right)_{E} + \left(\frac{\partial q_r}{\partial t}\right)_{AUT} \\ &+ \left(\frac{\partial q_r}{\partial t}\right)_{ACC} + \left(\frac{\partial q_r}{\partial t}\right)_{SED}.\end{aligned} \tag{6}$$

ρ_a denotes the air density and δ_i the Kronecker symbol whose value is specified in Subsection 2.2. Indexed terms in (3) to (6) represent the sources and sinks due to the microphysical processes and are defined below.

2.2. *Microphysical processes*

Microphysical processes operating in warm precipitation are of two categories. The first, contributing to the growth of droplets and raindrops, includes condensation and coalescence; the second, hindering this growth, comprises evaporation, break-up by collision and spontaneous break-up. All these processes, which are explicitly taken into account in the MDM are summarized hereafter. Their detailed description can be found in Appendix A (Section 8).

Cloud droplets are initiated in supersaturated air by activation of cloud condensation nuclei. The rate of activation of these nuclei ($(\partial n_{ac}/\partial t)_{ACT}$ in (4)) is a function of supersaturation. These cloud droplets are assumed to be produced at the rate $(\partial n_i/\partial t)_{ACT}$ in the smallest size category, so that $\delta_1 = 1$ and $\delta_i = 0$ for $i > 1$ in (3). The term $(\partial n_i/\partial t)_{CE}$ in (3) represents the variation of the number concentration of i-drops due to the condensation/evaporation process. The rate of growth of a droplet by diffusion of water vapour is deduced from the expression given by Mason (1971), assuming that effects of salt content, surface curvature and ventilation are negligible. The same expression is used to determine the decrease of size of a droplet by evaporation; however, evaporation is assumed to be instantaneous when the radius of the droplet becomes less than 1 μm which is the radius of the smallest size category. The overall rate of condensation/evaporation is represented by $(\partial q_v/\partial t)_{CE}$ in (2) and the diabatic effect on temperature due to the subsequent release or absorption of latent heat by $(\partial T/\partial t)_{CE}$ in (1). The coalescence and break-up processes resulting from collisions of drops are represented in the model following Brazier-Smith et al. (1973): collisions between an i-drop and j-drops result either in coalescence of all drops or in break-up of the i-drop with a j-drop producing then three identical satellites. These processes constitute sinks for the ith and jth categories and sources for higher (coalescence) or lower (break-up) size categories. They are represented by $(\partial n_i/\partial t)_{CC}$ and $(\partial n_i/\partial t)_{CB}$ in (3). The combined action of these processes tends to produce an equilibrium state in the distribution of hydrometeors. The term $(\partial n_i/\partial t)_{SB}$ in (3) represents the contribution of spontaneous break-up in modifying the size distribution of raindrops. This break-up results from deformation and hydrodynamic instability of very large raindrops during their fall through the air. The concentration of drops is also modified by their sedimentation; this contribution, denoted $(\partial n_i/\partial t)_{SED}$ in (3), is given by the vertical gradient of the flux of raindrops.

In a parameterized scheme, the effects of the microphysical processes above described are implicitly or explicitly taken into account with different degrees of sophistication and in a manner compatible with the representation of condensed water; this is done by assuming an analytical function for the size distribution of raindrops. Various microphysical parameterizations can be found in cloud physics literature; the parameterization of Kessler (1969) is chosen in the present study. So the following assumptions concerning the condensation/evaporation process are made in the MPM case: no supersaturation is allowed in rising air so that all the excess of water vapour above the saturation value is condensed; in subsaturated air, the cloud water evaporates in order to maintain the saturation. This process is represented by the fourth term in (5). When subsaturation is still present after all the cloud water has been evaporated, rain water is to be partially evaporated. The other processes responsible for the variation of rain water mixing ratio are autoconversion of cloud water into rain water and accretion of cloud water by raindrops; they are denoted $(\partial q_r/\partial t)_{AUT}$ and $(\partial q_r/\partial t)_{ACC}$ respectively in (5) and in (6). The sedimentation of rain water ($(\partial q_r/\partial t)_{SED}$ in (6)) is taken as the vertical flux of rain water. In the parameterization proposed by Kessler (1969), the above mentioned terms are expressed by considering an exponential size distribution for raindrops (Marshall and Palmer, 1948, hereafter referred to as MP). Their formulation is also given in Appendix A (Section 8).

3. Numerical procedure

The system of continuity equations ((1) to (6)) is solved time dependently. The sequence of computations consists of the following steps: (i) horizontal and vertical advection of air parcel and drops by taking account of the fall velocity of drops; (ii) estimation of the effect of the diabatic condensation/evaporation process on the vertically advected parcel; (iii) computation of the new drop size distribution resulting from the action of microphysical processes. Eddy diffusion terms are not explicitly considered in the present study; however, a weak diffusional effect is implied by the numerical scheme used in the computation of the advection terms.

3.1. *Advection scheme*

The advection terms of (1) to (6) are computed following a scheme which is based on upstream interpolation with cubic splines (Purnell, 1976). The low diffusional effect and the good computational performance (Long and Pepper, 1981) make this scheme attractive for the present purpose. The advective scheme has been chosen instead of the conservative scheme also proposed by Purnell (1976), for its better phase and amplitude fidelity; according to Ziegler (private communication), the conservative scheme appears to be affected by a weak instability and to yield an unacceptable solution.

The choice of grid spacing has to be adapted to the wind field used in the simulation. In this case study, the wind field (presented in Section 4) is characterized by strong updraughts (reaching 10 m s^{-1}) of limited horizontal extent of about 5 km and weak positive and negative vertical velocities (-1 to 3 m s^{-1}) elsewhere. Hence, the sensitivity of the retrieved fields to the grid spacing has been evaluated by using the MPM. The results show that mesh sizes as short as 250 m are required in the region of limited extent characterized by strong ascent of the airflow. In the present case, the horizontal mesh size varies according to a geometric progression, from 200 m to 1000 m and the vertical mesh size is constant at 250 m. The dimensions of the domain being 32 km long and 7.75 km high, this gives 80 grid points horizontally and 32 grid points vertically. This variable grid can be easily adapted to another wind field. The time step for horizontal advection terms is taken as $dt_A = 8$ s after testing; using an explicit fractional time step composition as in Purnell (1976), vertical advection terms are computed with the time step $dt_M = 4$ s, compatible with that of the microphysical computation.

3.2. *Boundary conditions*

Boundary conditions are applied for the computation of the advection terms at the inflow boundaries and at the ground. In the present case, the left side of the domain is an inflow boundary at all altitudes with no vertical velocity; thus the boundary values, specified from a radiosounde sounding, remain constant during the simulation. At the other inflow boundaries and at the ground, the values are progressively adapted to the nearest interior values with an appropriate response time. The scheme used inside the domain can be applied at the outflow boundaries.

3.3. *Computation of the supersaturation field*

The condensation process is accompanied by the release of latent heat. Since the supersaturation $(S-1)$ is related to the temperature and the water vapour mixing ratio values, the treatment of the supersaturation must be compatible with that of thermodynamic quantities. The explicit method for solution of the supersaturation field is not suitable for the present model because it requires a very small time step (Arnason and Brown, 1971). Thus, an implicit method analogous to that described by Hall (1980) is used in the present study. In the MDM, the amount of water condensed during a time step and the diabatic effect on temperature are first evaluated by integrating (A.2) with $S-1=S^*-1$ where S^*-1 is the value of the supersaturation obtained after advection of the air parcel. The supersaturation is then solved by iteration and used to explicitly compute the growth of droplets. In the MPM, the amount of water vapour condensed in order to maintain the saturation and the consequent variation of temperature are evaluated; the adjustment of the water vapour mixing ratio to its saturated value is obtained by performing iterations on the temperature value. A treatment identical to that used in the MDM is applied to evaluate the deficit of water vapour and the evaporation rate in subsaturated regions in both models. According to a sensitivity study, this method allows a time step $dt_M = 4$ s.

3.4. *Microphysical scheme*

Since microphysical processes modify size distribution of drops and mixing ratios, as shown by (3), (5) and (6), it is necessary to redistribute the new liquid water content among the size categories. In the MPM, a simple procedure can be used because there are only two categories. So, in this case, an Euler forward scheme is applied to (5) and (6) to integrate the terms $(\partial q_c/\partial t)_{CE}$ and $(\partial q_r/\partial t)_E$, as well as the terms relative to the autoconversion and accretion processes. In the MDM, because of the high number of size categories, a more sophisticated treatment is necessary to redistribute liquid water among the size categories, respecting the conservation of both the mass of liquid water and the number of drops.

The algorithm used to redistribute drops among size categories is essentially the same as in Kovetz and Olund (1969), with some minor modifications required by the present model. This algorithm is described in detail in Appendix B (Section 9). The main advantages of Kovetz and Olund's method are its very good conservation of water mass and number of drops and relatively small computation time compared to other schemes. Its main disadvantage is the spreading of the distribution towards the higher categories, which accelerates the formation of rain (Reinhardt, 1972). Since redistribution functions used in this study (see Appendix B) depend on the width of size categories, it was necessary to test the sensitivity of the method to this parameter and to evaluate its effect on numerical spreading. In order to cover the wide range of particle sizes involved in the processes described in Subsection 2.2, each size category is represented by a mean radius defined on a logarithmic scale by $r_i = r_1 \cdot 10^{(i-1)\mathrm{Dr}}$ where Dr is given by $\mathrm{Dr} = (\log(r_N) - \log(r_1))/(N-1)$ with $r_1 = 1\ \mu\mathrm{m}$ and $r_N = 5000\ \mu\mathrm{m}$. The method was tested for three numbers of size categories: $N = 25$, $N = 50$ and $N = 75$, each corresponding to a given width of size categories according to the expression of Dr above given. The test was made with a 1-D version of the MDM in the case of an ascending air parcel with conditions of simulation identical to those given by Ochs (1978) (Section 9, case 1 in his paper). Reflectivity values deduced from the present method during the ascent of the air parcel were compared to those obtained by Ochs (1978) from a higher order scheme which minimizes numerical spreading (Ochs and Yao, 1978). The results of this test show that: (1) numerical spreading decreases with increasing value of N; (2) the method is comparable in performance to Ochs and Yao's method for identical width of size categories, which is the case when $N = 75$ in the present method. In the case $N = 50$, the relative dispersion of the simulated size distribution, defined as the ratio of the standard deviation to the mean diameter, has been compared with the relative dispersion from spectra observed during the PAP 79 experiment (Personne, 1983). Fig. 1 represents the relative dispersion in both cases as a function of altitude above the cloud base. The relative dispersion deduced from the simulation (solid line) is less than that deduced from measurements (symbols) at all altitudes. Hence, numerical errors in the present scheme do not unduly accelerate the development of large raindrops, and it can be used to simulate the rain formation. Considering both the computational storage and the results of the above tests, the value of 50 has been chosen for N in the present study.

4. Description of the squall line

The event considered in this study is a squall line observed on 22 June 1981 at Korhogo in the North of Ivory Coast during the COPT 81

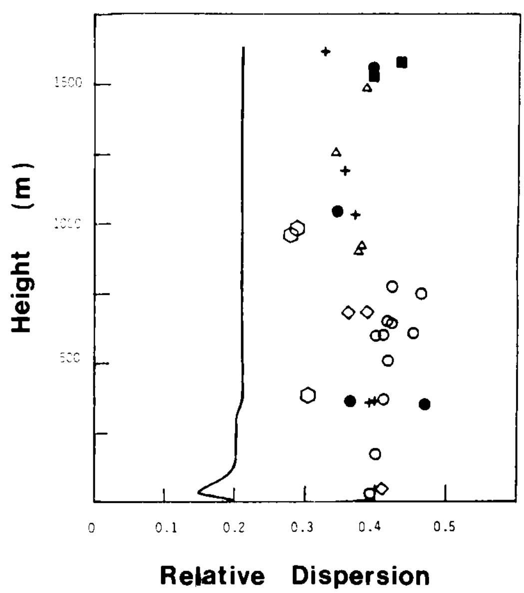

Fig. 1. Relative dispersion of the size distribution of drops as a function of altitude above cloud base deduced from the simulation (solid line) and from measurements during the PAP79 experiment (symbols).

experiment; it has been fully described and analysed in Roux et al. (1984); only the main features are reviewed below. Two distinct regions of radar reflectivity were observed: a convective region of intense precipitation at the front part of the system and a stratiform region of weaker precipitation at the rear. At the ground, these regions were respectively of extent 50 km and 200 km along the propagation axis. These features were almost steady during the displacement of the squall line at 19 m s^{-1} over the experimental site. A dual Doppler radar system performed measurements in the convective part of the system. The analysis of the data revealed a steady quasi two-dimensional structure of the wind and reflectivity fields. Equivalent two-dimensional wind and reflectivity fields were determined for this convective part in the vertical plane along the propagation axis by Hauser and Amayenc (1986). These fields at 0418 GMT are represented in Fig. 2. Two opposing airflows are present: a rearward flow entering the system at all altitudes, and a forward flow at low levels. Fig. 3 shows the vertical profile of temperature and humidity of the atmosphere at 0348 GMT at Korhogo, i.e., 30 mn before the arrival of the squall line over the experimental site. This profile reveals a moderate instability of the air in the lower levels (below 1200 m altitude). The analysis given by Roux et al. (1984) suggests that the cold forward flow, coming from the stratiform region lifted up the air ahead and initiated strong updraughts reaching 10 m s^{-1}. The water loading resulting from differential sedimentation of precipitation water weakened the updraughts, which is shown by the existence of very small vertical velocities for 12 km $\leqslant x \leqslant$ 17 km and $z \geqslant 3$ km in Fig. 2. Intense precipitation, corresponding to reflectivity values greater than 50 dBZ was observed just beneath this zone. The convective updraughts were seen to strengthen again for $x > 17$ km and $z \geqslant 3$ km with moderate intensity. Some weak downdraughts (less than 1 m s^{-1}) are observed at the transition zone between the forward flow and the rearward flow. Some features of the equivalent reflectivity field such as the oscillations of the contours around $z = 5$ km or the horizontal extent of the core $Z \geqslant 50$ dBZ for $x \geqslant 13$ km are transient since they do not appear on successive sequences of radar data. According to Hauser and Amayenc (1986), no bright band was evident in the convective region and most of the precipitation was formed below $z = 6$ km corresponding to the -10°C isotherm. These observations suggest that the precipitation in the convective region was mainly produced through warm microphysical processes. The domain used for the present simulations is delimited by the thick line in Fig. 2. The wind field given in this domain has been

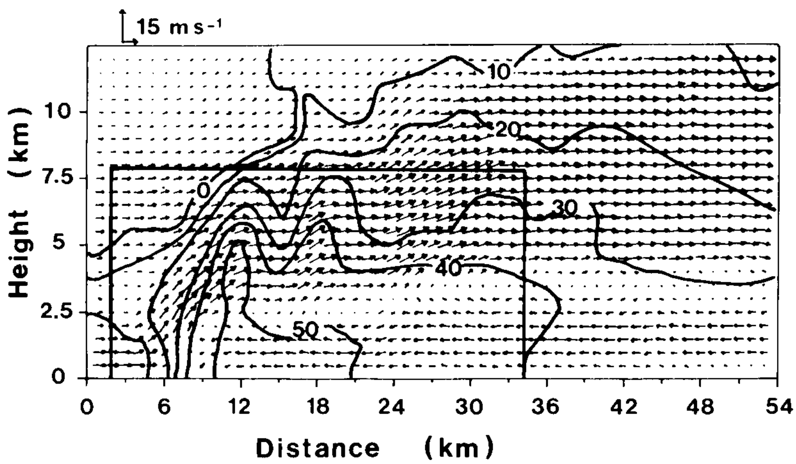

Fig. 2. Two-dimensional fields of wind (m s^{-1}) and reflectivity (dBZ) deduced from the Doppler radar observations at 0418 GMT in the convective part of the 22 June 1981 squall line (from Hauser and Amayenc, 1986). The 0°C and -10°C isotherm levels are indicated. The heavy solid line delimits the domain used for the simulations.

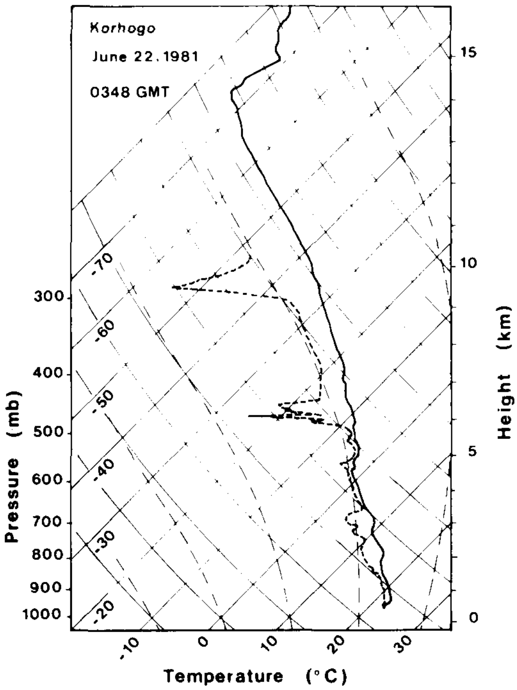

Fig. 3. Vertical profile of temperature and humidity deduced from a radiosounding of the atmosphere at Korhogo on 22 June 1981 at 0348 GMT.

interpolated on the irregular grid mentioned in the previous section. The 0348 GMT radiosounding is used to initialize temperature and humidity fields.

5. Results and discussion

Simulations were performed with both versions of the model. The microphysical fields reached a nearly steady state after 45 mn of simulation in the MDM case and 25 mn in the MPM case. A fairly good agreement was found in the region of intense precipitation, between the simulated results and available observations of reflectivity and rainfall rate at the ground. The details of this comparison will be seen in Subsection 5.3. In order to compare the two sets of simulated results, cloud and rain water mixing ratios as well as autoconversion and accretion rates are computed from the drop size distribution of the MDM by taking a radius of 100 μm as the division between cloud droplets and raindrops. The sensitivity of the model results to the microphysical scheme is examined in Subsection 5.1 by comparing fields retrieved from both versions, and in Subsection 5.2 where water budget results are presented. The characteristics of some size distributions are analyzed in Subsection 5.4.

5.1. *Formation of rain*

The cloud water and water vapour deficit mixing ratios are shown in Fig. 4a (MDM case) and Fig. 4b (MPM case). While the region of high cloud water content ($q_c > 1$ g kg^{-1}) coincides in both cases with the ascending flow described in Section 4, the cloud water mixing ratio reaches higher values in the MDM case than in the MPM case. Subsaturated air in Fig. 4a roughly corresponds to the forward flow (see Fig. 2). The deficit is generally less than 1 g kg^{-1}, which corresponds to a relative humidity of 95% to 99%; it reaches higher values in zones of weak downdraughts due to the effect of adiabatic warming. These characteristics are also observed in Fig. 4b, but the deficit is less important than in the previous case, and most of the forward flow is saturated. This indicates that evaporation of rain in the forward flow is more important in the MPM case than in the MDM case. This point will be examined in Subsection 5.2.

Fig. 5 represents the rain water mixing ratio in the MDM case and in the MPM case respectively, in the domain limited by $x = 24$ km, because the most intense precipitation is formed in this part of the system. The maximum rain water mixing ratio is located 3 to 4 km behind the corresponding maximum of cloud water content; it reaches 6 g kg^{-1} in the MDM and only 4 g kg^{-1} in the MPM. The "comma" shape of rain water contours is due to the combined action of advection and evaporation in the forward airflow behind the gust front (see Figs. 2, 4). The higher rain water content for $x \leqslant 8$ km in Fig. 5b than in Fig. 5a shows a faster conversion of cloud water to rain water in the MPM case than in the MDM case.

The conversion of cloud water to rain water is the product of autoconversion and accretion processes. The autoconversion rate is presented in Fig. 6. The main difference between Figs. 6a, 6b is that high autoconversion rate affects a larger extent in (b) than in (a), especially for 6 km $\leqslant x \leqslant$ 8 km. In the MPM, the autoconversion rate is a linear function of difference

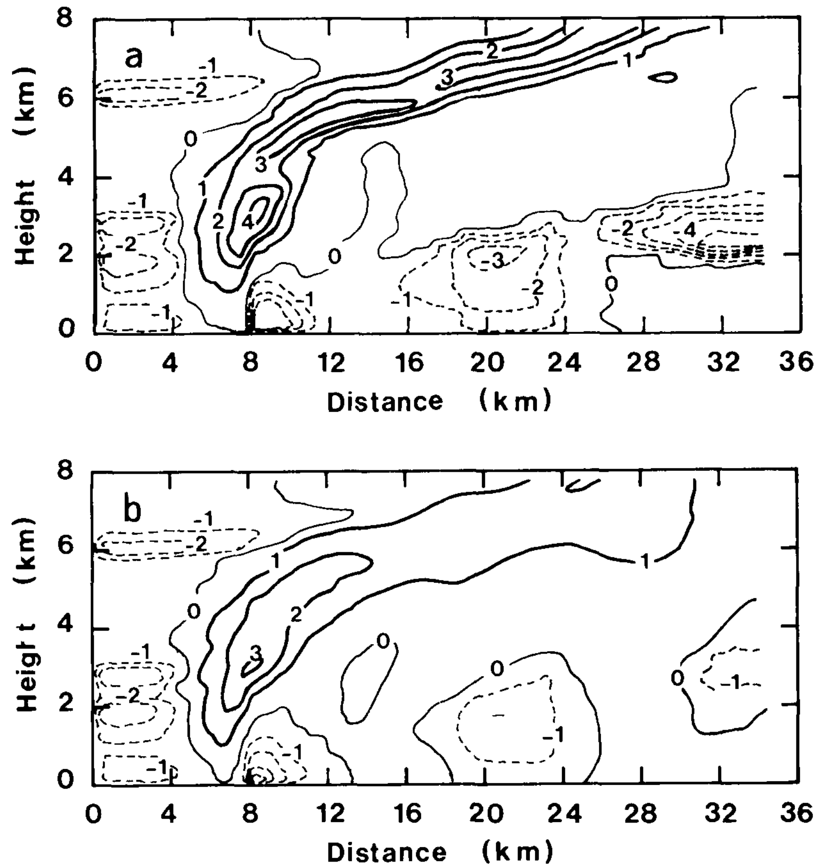

Fig. 4. Field of cloud water (solid line) and water vapour deficit (dashed line) mixing ratios (g kg^{-1}) deduced from the detailed model (Fig. 4a) and from the parameterized model (Fig. 4b).

between the cloud water content and a threshold value. Therefore, the extent of the zone of high autoconversion as well as the shape of the contours in Fig. 6b depend on the characteristics of the corresponding cloud water field (Fig. 4b). In the MDM, the autoconversion is not related to a threshold value of q_c, but rather to the presence of large cloud droplets, necessary to enhance coalescence and produce raindrops. According to results of test simulations, such large cloud droplets ($r_i = 50$ μm) need 100 s to 200 s to be produced. Because of this time delay and advection, these large droplets only appear in the region $x \geqslant 8$ km. As soon as these large droplets appear, the autoconversion rate becomes very efficient because of the high cloud water content in this region.

The accretion rate is presented in Fig. 7. The accretion process contributes to the greater rate of production of rain in the MDM than in the MPM for $x > 8$ km, as shown by the greater values in Fig. 7a than in Fig. 7b. Indeed, the higher cloud water content observed in Fig. 4a than in Fig. 4b may explain part of the difference. But the accretion process is also a function of the size distribution of rain since, for a given rain water content, the volume swept-out by the raindrops increases with decreasing mean radius of their size distribution. In the zone of intense accretion, mean radii deduced from the MDM are smaller than those deduced from assumed MP distributions because of the presence of large concentrations of small raindrops in this zone.

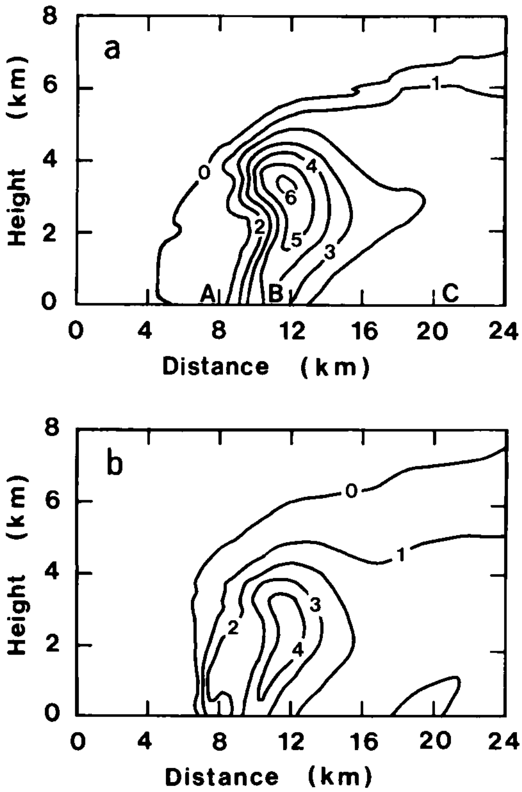

Fig. 5. Field of rain water mixing ratio (g kg^{-1}) deduced from the detailed model (Fig. 5a) and from the parameterized model (Fig. 5b). The location of the spectra shown in Fig. 10 is indicated by the letters A, B, C in Fig. 5a.

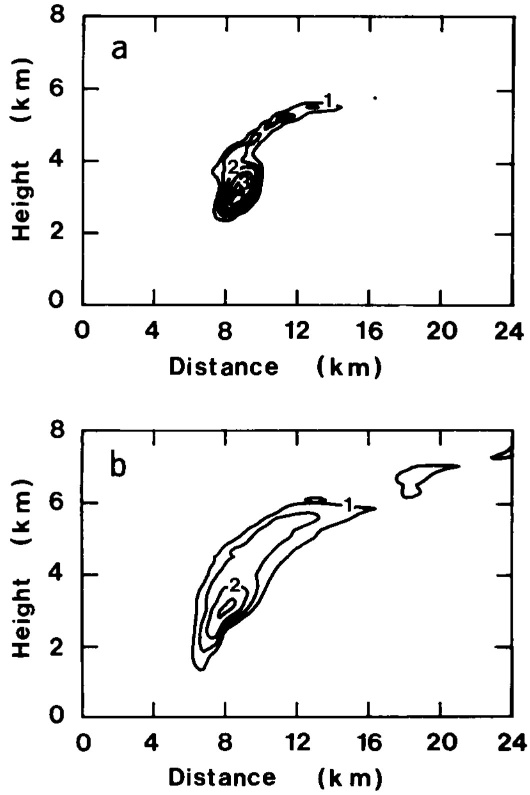

Fig. 6. Autoconversion rate (10^{-3} g kg^{-1} s^{-1}) deduced from the detailed model (Fig. 6a) and from the parameterized model (Fig. 6b); contours interval is $0.5 \cdot 10^{-3}$ g kg^{-1} s^{-1}.

5.2. Water budget

In the case of near steady state of liquid water fields, the amount of condensed water in a given domain should be balanced by the amounts of precipitated rain water at the ground, advected cloud water and rain water, evaporated cloud water and rain water. These terms have been computed as averages over 720 s once quasi-stationary fields have been reached. All the terms have been evaluated for seven domains of increasing sizes; these domains are all 7.75 km high and they are horizontally delimited by $x_f = 0$ km (front edge) and respectively by $x_r = 6$, 8, 10, 12, 14, 16 and 21 km (rear edge). They are referred to as (x_f, x_r) in the text. Results of the water budget for some of these domains are presented as percentages of liquid water (Table 1) or of condensation rate (Tables 2, 3).

The partitioning of liquid water into cloud water and rain water (Table 1) and the precipitation efficiency representing the amount of precipitated water at the ground (Table 2) are very different from one model to the other for the domain (0, 8). The difference between both sets of values is much smaller for the domain (0, 14) which includes all the zone of strong updraughts, and vanishes for the domain (0, 21) with 70.1% of precipitation efficiency in the MDM and 69.5% in the MPM. These results show that the difference in production of rain water and precipitation efficiency between both models is confined to the front edge of the region of strong

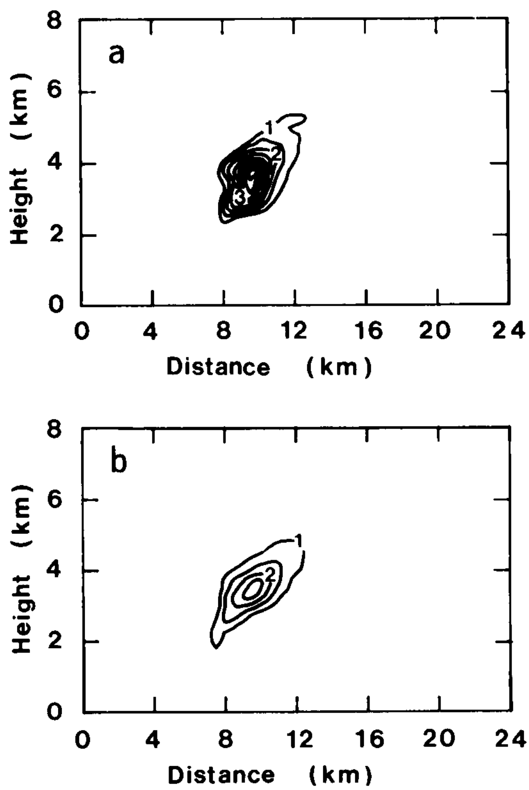

Fig. 7. Accretion rate (10^{-2} g kg^{-1} s^{-1}) deduced from the detailed model (Fig. 7a) and from the parameterized model (Fig. 7b); contours interval is $0.5 \cdot 10^{-2}$ g kg^{-1} s^{-1}.

updraughts and that the global production of rain is not sensitive to the microphysical scheme. They confirm that the production of rain is faster in the MPM than in the MDM at front of the system.

The water budget for this squall line has also been investigated from experimental data by Chong (1983) and Hauser et al. (1984). Their results cannot be directly compared to the present ones because the domains involved are not the same as those defined above. However, it can be remarked that Hauser et al. (1984) found a precipitation efficiency of 69.2% for a domain 26 km long and 6 km high including the region of strong updraughts and the zone of intense precipitation; this efficiency is in good agreement with the efficiency of about 70% given above for the domain of comparable size (0, 21).

In Table 3 are given the amounts of advected cloud water and rain water (1st to 4th line), and evaporated cloud and rain water (5th and 6th line, respectively) for the domain (0, 21). Because of the characteristics of the above wind field, net advection of water at $x_r = 21$ km includes advection of both cloud and rain water towards the rear of the system above $z = 2.5$ km and inward advection of only rain water below this altitude. The budget of advected water is almost the same in both cases. Advection of condensed water as cloud (about 19%) and rain (22.5% in

Table 1. *Ratios of cloud water content to total liquid water content and of rain water content to total liquid water content given by the detailed model (MDM) and by the parameterized model (MPM) for the domains (0, 8), (0, 14) and (0, 21)*

	$x_r = 8$ km		$x_r = 14$ km		$x_r = 21$ km	
	MDM	MPM	MDM	MPM	MDM	MPM
Ratio of cloud water (%)	89	66	34	33	30	31
Ratio of rain water (%)	11	34	66	67	70	69

Table 2. *Precipitation efficiency given by the detailed model (MDM) and by the parameterized model (MPM) for the domains (0, 8), (0, 14) and (0, 21)*

	$x_r = 8$ km		$x_r = 14$ km		$x_r = 21$ km	
	MDM	MPM	MDM	MPM	MDM	MPM
Precipitation efficiency (%)	5.2	12.3	62.4	65.4	70.1	69.5

Table 3. *Sinks of cloud and rain water (see text) expressed as percentages of the condensation rate, given by the detailed model (MDM) and by the parameterized model (MPM) for the domain (0, 21)*

	$x_r = 21$ km	
	MDM	MPM
Net advected cloud water (%)	19.0	19.5
Net advected rain water (%)	10.0	5.4
Outwards advected rain water (%)	22.5	17.2
Inwards advected rain water (%)	12.5	11.8
Evaporated cloud water (%)	0.6	1.5
Evaporated rain water (%)	0.9	5.5

the MDM and 17.2% in the MPM) towards the rear, contribute to the production of rain beyond $x_r = 21$ km. The small difference in the outward advected rain water between both models is due to the presence of a larger rain water content for $z > 5$ km in the MDM case than in the MPM case (Fig. 5). At this altitude, rain water is mainly formed by small raindrops suspended into the ascending airflow; the assumption of an MP distribution for rain and the use of (A.12) in the MPM tend to overestimate the precipitation of rain water in this region and thus to reduce the local rain water content. Evaporated cloud water is very small compared to the other terms of the water budget. Evaporation of rain takes place in the unsaturated air associated with small downdraughts (Figs. 2, 4). In the MDM, it varies from 10^{-5} g kg^{-1} s^{-1} to $3 \cdot 10^{-4}$ g kg^{-1} s^{-1}; the corresponding diabatic cooling rate varies from 0.08 K hr^{-1} to 0.2 K hr^{-1}. The rates obtained in the MPM are ten times greater than these values. In the MDM case, evaporation of small raindrops takes place in the upper part of subsaturated air; once these small raindrops are evaporated, the rate of evaporation decreases since the remaining rain water is distributed into the large size categories. In the MPM case, large concentrations of small raindrops are continuously and artificially produced because of the assumption of an MP distribution, which gives a large rate of evaporation all across the forward flow and holds the air nearer to saturation (Fig. 4b).

The above results confirm that the efficiency of production of rain is sensitive to the microphysical scheme in the region of strong updraughts. Moreover, they show that the rate of evaporation of rain water is significantly overestimated in the parameterized case. A correct assessment of the evaporation of rain water is important since the downward motions observed in precipitating systems are often partly induced by the cooling due to evaporation of rain.

5.3. *Comparison with the observational data*

The available observational data are the mean reflectivity field deduced from the dual Doppler radar data and the rainfall rate at the ground given by a rain gauge situated in the region observed by the radars.

Fig. 8 represents the reflectivity field deduced from the MDM and MPM respectively, and Fig. 8c the mean reflectivity field deduced from

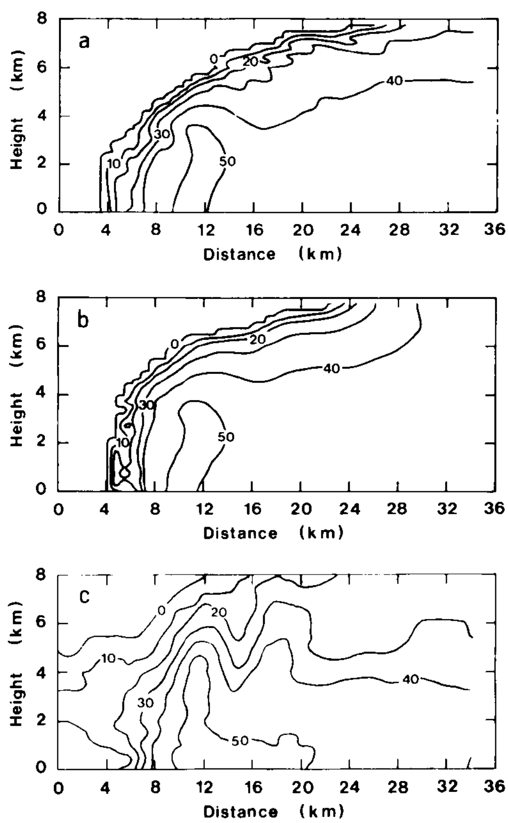

Fig. 8. Reflectivity field (dBZ) deduced from the detailed model (Fig. 8a) and from the parameterized model (Fig. 8b). Mean reflectivity field (dBZ) deduced from Doppler radar measurements (Fig. 8c).

Doppler radar measurements. Both models are able to recover the core of high reflectivity ($Z \geqslant 50$ dBZ) observed for 10 km $\leqslant x \leqslant$ 13 km, the global shape of the contours and their gradient. However, when considering some details such as the shape of the contours for 4 km $\leqslant x \leqslant$ 5 km, especially the contour $Z = 20$ dBZ, the agreement with the observed field is better in the MDM case than in the MPM case. Because of steady state assumption, the model cannot reproduce transient features such as the oscillations of the Z contours around $z = 5$ km or the horizontal extent of the core $Z > 50$ dBZ for $x > 13$ km. Simulated fields do not agree very well beyond $x = 16$ km where the reflectivity is overestimated, especially in the MPM case (Fig. 8b). This may be due to the fact that part of the precipitation water present in this region is initiated above the -10°C isotherm level where ice particles may coexist with cloud water, so that the assumption of only warm microphysics might not be adequate to recover precipitation for $x > 16$ km.

Fig. 9 shows the rainfall rate at the ground measured by the rain gauge and deduced from both versions of the model (see legend) as a function of both space and time. Both models are able to retrieve the intense precipitation observed at the ground, although the simulated maxima are slightly lower than the observed maximum. The agreement concerning the location of the peak is better in the MDM case than in the MPM case: in this latter case, the peak appears 30 s earlier, which corresponds to a distance of 600 m. This distance is relatively large compared to the 3 km width of the zone of intense updraughts which have produced this peak of precipitation. Thus the MDM seems to give better results than the MPM in the convective zone. Additional comparisons with other observational data, not available in the present case study, would yet have been very useful to confirm this result.

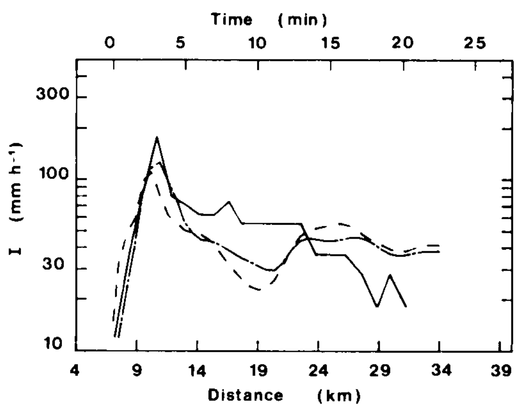

Fig. 9. Rainfall rate (I) at the ground (mm hr^{-1}) measured by a rain gauge (solid line), deduced from the detailed model (dash-dotted line) and from the parameterized model (dashed line), as a function of distance (km) or time (mn).

5.4. *Size distributions of raindrops*

While in the MPM size distributions of raindrops are constrained to be exponential, in the MDM they result from the action of advection and various microphysical processes incorporated in the model, and are supposed to reproduce real size distributions. Size distributions obtained in the MDM simulation can be compared to "in situ" measurements of raindrop spectra when these are made; this provides an additional means to validate the model. In the present case, this comparison cannot unfortunately be performed because in situ measurements are not available. However, the analysis of raindrop spectra simulated by the MDM in conjunction with the wind field of the system can supply useful information about the combined effect of microphysical processes, differential sedimentation and advection on these spectra. Three size distributions deduced from the MDM are presented in Fig. 10 as well as the MP relations (straight lines) and equilibrium spectra (dashed lines in cases B and C) corresponding to the same rain water content. These dashed-lined spectra represent the equilibrium state obtained by the spectrum when simulating the combined action of coalescence, break-up by collision and spontaneous break-up processes. The three size distributions are taken from different parts of the system; locations are indicated in Fig. 5a by the letters A, B, C. The first distribution (A) is located under the region of intense updraughts. It reveals an excess of large drops and a deficit of small drops compared to the MP straight line. A similar feature has been observed by Carbone and Nelson (1978) during the growth stage of convective storms. The deficit of small drops at the ground is a consequence of the strong updraughts which prevent them from falling.

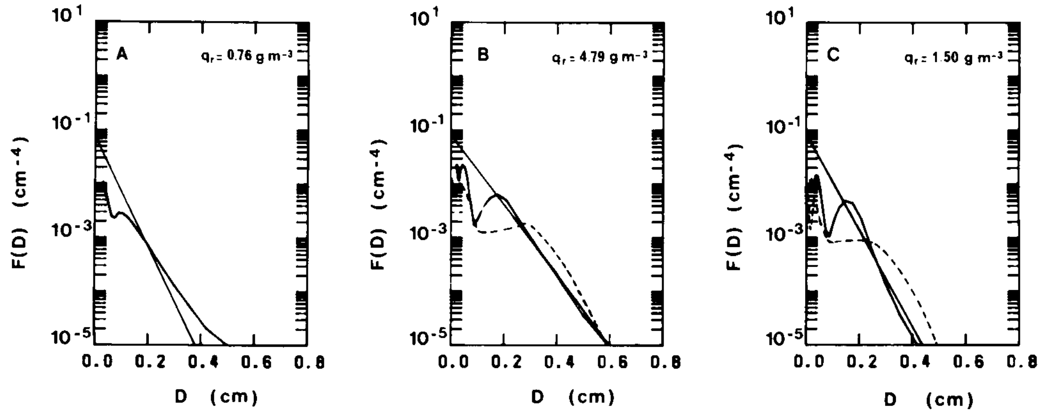

Fig. 10. Distributions of raindrops with diameter obtained by the detailed model. Their location is indicated by the letters A, B, C in Fig. 5a. The straight line represents the exponential law given by Marshall and Palmer (1948) and the dashed line (cases B and C) the equilibrium shape of the size distributions.

Raindrops large enough to fall grow by accretion of small drops in the cloud. Because of their small number, break-up by collision is not efficient enough to quickly modify the spectrum at large sizes. The second distribution (B) is obtained in the region of intense precipitation. The agreement with the MP relation is good for drops whose diameter D exceeds 0.2 cm, with a slight tendency for the computed distribution to be steeper than the MP slope. There is a deficit of drops for $D \leqslant 0.2$ cm compared to the MP relation. The last distribution (C) is located behind the region of intense precipitation. This distribution is not very different from the second one, but in this case, the slope for drops of diameter greater than 0.2 cm is much steeper than the corresponding MP relation. Such behaviour for large drops has also been observed by List and Gillespie (1976) in simulated size distributions. The depletion of drops for $D \leqslant 0.2$ cm is due to the combined effect of evaporation and coalescence; it may be also partly attributed to the scheme used to simulate break-up by collision since this depletion with a minimum at $D = 0.1$ cm is similar to that simulated by Brazier-Smith et al. (1973). In these two cases (B and C), drops originating from high-level regions characterized by weak updraughts undergo numerous collisions all along their fall. Subsequently coalescence and break-up tend to produce the equilibrium shape of the raindrop spectrum; in the present case, both size distributions are still far from their equilibrium shape. These three examples suggest that the processes which shape the size distribution are highly dependent on dynamic and thermodynamic characteristics of the region where drops have been formed as well as the elapsed time since leaving the cloud base, as discussed by Carbone (1985).

In order to examine all the spectra obtained at the ground in and behind the region of intense precipitation, a normalization procedure similar to that of Sekhon and Srivastava (1971) has been applied to every size distribution for $x \geqslant 10$ km. Normalized values are plotted in Fig. 11 as functions of normalized diameter D/D_0, D_0 being the median volume diameter; the normalized MP relation is also represented (straight line). The normalized size distributions deduced from the MDM display features similar to those experimentally obtained by Willis (1984): the density of small drops ($D/D_0 < 1$) is lower than the density given by the MP relation and the slope for big drops ($D/D_0 > 1$) is steeper than the MP slope. The normalized values can be fitted by the gamma distribution function: $F_{\text{norm}}(D/D_0) = 2092.4(D/D_0)^{5.23} \exp(-7.25 D/D_0)$; the numerical constants of F_{norm} have been determined using a least-squares method. This result shows that the raindrop spectra of moderate to intense precipitation with frequent coalescence and break-up of raindrops, tend to rapidly approach a gamma distribution when there is no continuous supply of small cloud droplets.

It is also interesting to examine the $Z-q_r$ relationship, since this relationship is often used to estimate the rain water content from the Z data. Hauser and Amayenc (1986), for example, explicitly used this relationship in their method of

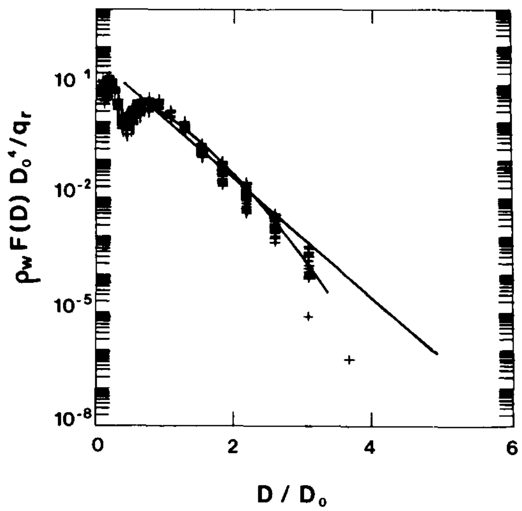

Fig. 11. Normalized size distributions at the ground for $x > 10$ km. the normalized relation of Marshall and Palmer (1948) and the relation $F_{\text{norm}}(D/D_0) = 2092.4(D/D_0)^{5.23}\exp(-7.25D/D_0)$ are also represented.

retrieval of microphysical fields. The $Z-q_r$ relationship deduced from the simulation with the MDM for the entire domain of simulation is represented in Fig. 12. This figure shows that a wide variety of reflectivity values can be obtained within one system for the same value of q_r. Rain water content $q_r \leqslant 1$ g m^{-3} is mainly found at the front edge of the precipitating system as shown in Fig. 5a; in this region, rain water is mainly distributed into small size categories at height and in large size categories near the ground (Fig. 10, case A). Consequently, almost identical values of rain water content at height and near the ground may correspond to quite different values of reflectivity (Fig. 5a and Fig. 8a), which produces the important dispersion of reflectivity values for a given value of $q_r \leqslant 1$ g m^{-3}. This dispersion is still observed for high values of q_r ($q_r \geqslant 3$ g m^{-3}) but it is less important than in the previous case because a large rain water content implies the presence of large raindrops and efficient coalescence and break-up.

Fig. 13 represents the $Z-q_r$ relationship deduced from the simulation with the MDM, at the ground (symbols Y) and at 3250 m altitude (symbols X). Also represented are the relation $\rho_a q_r = 0.072(Z/200)^{0.55}$ deduced by Marshall and Palmer (1948) from ground data (solid line), and

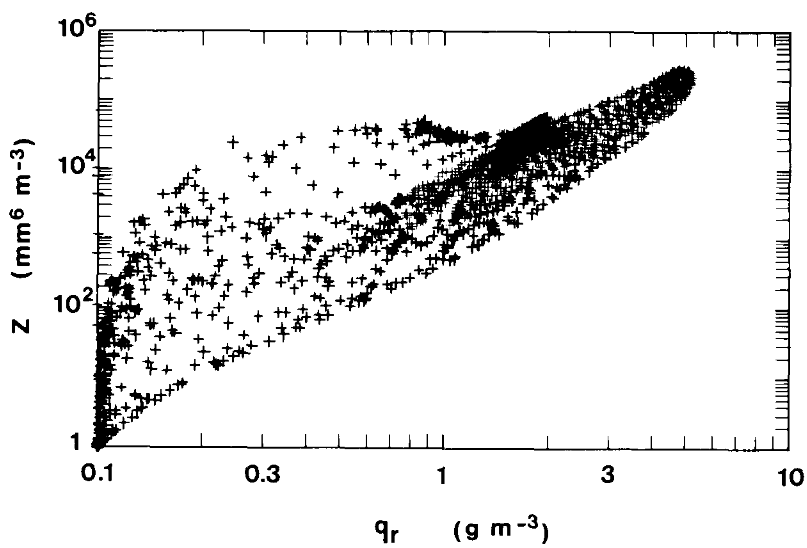

Fig. 12. Reflectivity values (mm^6 m^{-3}) versus rain water mixing ratio (g m^{-3}) in the case of the detailed model for the entire domain of simulation.

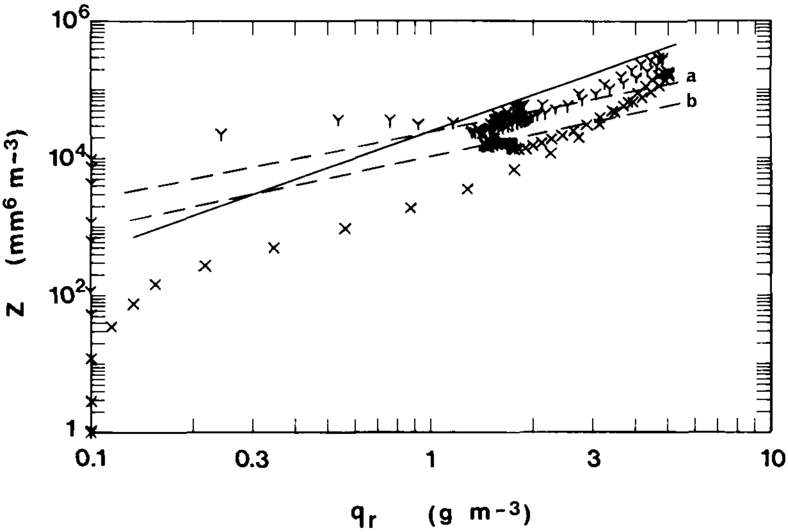

Fig. 13. Reflectivity values (mm^6 m^{-3}) versus rain water mixing ratio (g m^{-3}) in the case of the detailed model at the ground (Y) and at 3250 m altitude (X). The solid line represents the empirical $Z - q_r$ relation deduced by Marshall and Palmer (1948): $\rho_a q_r = 0.072(Z/200)^{0.55}$. The dashed lines represent the relation $Z = 4436 D_0^3 \rho_a q_r$ for $D_0 = 0.18$ cm (a) and for $D_0 = 0.12$ cm (b).

the relation $Z = 4436 D_0^3 \rho_a q_r$ deduced by integration from the function F_{norm} in two cases (dashed lines (a) and (b)). The dashed lines (a) and (b) respectively correspond to mean diameters $D_0 = 0.18$ cm or $D_0 = 0.13$ cm characterizing size distributions for $x > 14$ km at the ground or $z = 3250$ m. These lines approximate the (Z, q_r) symbols better than the MP $Z - q_r$ relation in the range 1 g m^{-3} $< q_r <$ 3 g m^{-3}, i.e., for $x > 14$ km and up to $z \sim 5$ km. However, the lines fail outside this range, especially for $q_r > 1$ g m^{-3}, because in the corresponding region (front edge of the precipitating system) size distributions are very different from a gamma distribution.

These results show that the presence of large raindrops is not only dependent on the rain water content but also on the dynamical conditions which influence the efficiency of microphysical processes producing raindrops, and that the complex relationships existing between microphysical parameters in a real precipitating system cannot be easily reproduced by simple relations.

6. Conclusion

This paper presents a method of retrieving microphysical fields based on the use of wind fields derived from Doppler radar data and on the solution of continuity equations. The sensitivity of the retrieval method to the microphysical scheme has been evaluated in the case of a tropical squall line observed during the COPT 81 experiment, by developing two versions of the model, one incorporating a complete description of warm microphysics and the other using the parameterization of Kessler (1969). Both models are able to reproduce radars and rain gauge observations of intense precipitation behind the strong updraughts, with a slightly better agreement in the case of the detailed model.

A sensitivity study was carried out by comparing the fields of cloud and rain water, the autoconversion and accretion rates. This comparison has shown that the general features of these fields are fairly insensitive to the microphysical scheme, suggesting that these features depend mainly on the dynamical characteristics of the squall line. However, a detailed analysis of the fields and results of a water budget calculation reveal that, in the region of intense updraughts, the efficiency of production of rain is quite sensitive to the microphysical scheme. Another aspect sensitive to the microphysical scheme is the rate of evaporation of rain because of the assumption of the MP distribution in the parameterized model. Indeed, in the forward flow of the squall line, the diabatic cooling due to this evaporation is more important in the parameterized model than in the detailed model. These results show that this discrepancy due to the choice of the microphysical scheme appears where microphysics may most significantly affect dynamical processes in clouds.

Rutledge and Hobbs (1983, 1984) and Ziegler (1985) have shown that the analysis of fields retrieved by a diagnostic model gives information about the microphysical processes leading to precipitation. This study shows that this information may depend on the degree of sophistication of the microphysical scheme incorporated in the model; further, this type of model provides a tool to evaluate the performance of various microphysical schemes. Simulated size distributions have been tentatively analysed from this point of view. This analysis showed that the size distribution of raindrops in moderate to intense precipitation may rapidly approach a quasi-equilibrium shape which can be approximated by a gamma distribution, while size distributions in weak precipitation do not approach such a quasi-equilibrium shape because of the relatively low number of coalescence and break-up events. This kind of result should be analysed in future with respect to in situ measurements of raindrop size spectra.

The present study has to be carried on in several ways. It is necessary to perform sensitivity tests in order to evaluate the effect of possible wind fields errors on the retrieved fields since it was shown that these fields are conditioned by the kinematic characteristics of the system. Moreover, a complete description of microphysical processes operating in the squall line needs the ice phase to be introduced in the detailed model. This would give information about the processes acting in the stratiform part and the interaction between the convective and the stratiform parts. Sensitivity studies similar to that developed in this paper would help to improve parameterizations.

7. Acknowledgements

The authors are indebted to Dr. R. G. Soulage for his helpful comments and criticisms. They are grateful to Dr. Y. Pointin who offered useful suggestions during this research and provided drawing programs. They appreciate the comments of two reviewers who helped to improve the original manuscript. Many thanks are also due to Drs. D. Hauser and P. Amayenc who provided part of the data. Mrs. J. Squarise and O. Guillot contributed to the presentation of the manuscript. The calculations were performed on the NAS 9080 and the IBM 3090 computers of the CIRCE. This research was supported by the Institut National des Sciences de l'Univers under contract ATP.RA 56-34 and by the Direction des Recherches Etudes et Techniques under contract no. 86.34.056.470.75.01.

8. Appendix A

This Appendix completes the brief description of microphysical processes and gives the expression of indexed terms of (1) to (6).

8.1. MDM case

The number concentration of active cloud condensation nuclei n_{cc} is given by a function of the saturation ratio S:

$$n_{cc} = c(S-1)^k, \tag{A.1}$$

where c and k are empirical constants. The value of c and k are respectively taken as $2 \cdot 10^8$ m^{-3} and 0.5. Such values characterize maritime air (Twomey and Wojciechowski, 1969) and are chosen in the present study because the simulated cloud is formed in such an air mass of the West African monsoon. The saturation ratio S is defined as $S = q_v/q_s$ where q_s is the saturation mixing ratio. The rate of activation of these nuclei, $(\partial n_{ac}/\partial t)_{ACT}$ in (4) is computed following the method proposed by Hall (1980): new nuclei are activated when the number n_{cc} given by (A.1) is greater than the number n_{ac} of previously activated nuclei, and their number equals the difference $n_{cc} - n_{ac}$. The rate of growth of a droplet of radius r_i by diffusion of water vapour is computed according to Mason (1971). It is given by:

$$\left(\frac{dr_i}{dt}\right)_{CE} = \frac{S-1}{r_i \rho_w \left\{ \dfrac{L}{K_a T}\left[\dfrac{LM}{RT} - 1\right] + \dfrac{RT}{DMe_s} \right\}}, \tag{A.2}$$

where ρ_w is the density of liquid water; L denotes the latent heat of condensation, M the molecular weight of water, R the universal gas constant, K_a the thermal conductivity of the air and D the diffusion coefficient of water vapour in air. The overall rate of condensation/evaporation thus gives:

$$\left(\frac{\partial q_v}{\partial t}\right)_{CE} = -\frac{\rho_w}{\rho_a}\sum_{i=1}^{N} 4\pi r_i^2 n_i \left(\frac{dr_i}{dt}\right)_{CE}$$

and the diabatic effect on temperature due to the subsequent release or absorption of latent heat is given by:

$$\left(\frac{\partial T}{\partial t}\right)_{CE} = -\frac{L}{C_p}\left(\frac{\partial q_v}{\partial t}\right)_{CE}$$

where C_p is the specific heat of air at constant pressure.

The number of j-drops which collide with a larger i-drop per unit time is given by:

$$NC(i, j) = \pi(r_i + r_j)^2 E_{ij}(V_i - V_j) n_j, \tag{A.3}$$

where V_i and V_j represent the terminal velocities of the i-drop and the j-drop, respectively, and E_{ij} the collision efficiency. If $P_{CC}(i, j)$ is the probability that all collisions occurring during the time step dt result in coalescence, the number $n_i P_{CC}(i, j)$ of i-drops grows by coalescence with a rate given by:

$$\left(\frac{dr_i}{dt}\right)_{CC} = \frac{1}{4\pi\rho_w r_i^2}\sum_{j=1}^{i} m_j NC(i, j) \tag{A.4}$$

where m_j represents the mass of the j-drop. The probability that at least one collision between a j-drop and the i-drop results in separation and break-up is $1 - P_{CC}(i, j)$. So, the remaining $n_i(1 - P_{CC}(i, j))$ drops are supposed to undergo separation and break-up during the time step dt. Following Brazier-Smith et al. (1973), these i-drops and j-drops contribute equally to the production of three identical satellite drops whose radius $r_{s_{ij}}$ is given by:

$$r_{s_{ij}} = \left[\frac{0.04 r_i^3 r_j^3}{r_i^3 + r_j^3}\right]^{1/3}. \tag{A.5}$$

The radii of i-drops and j-drops are consequently modified; they are given by:

$$\begin{aligned} r_{ij} &= (r_i^3 - 1.5 r_{s_{ij}}^3)^{1/3}, \\ r_{ji} &= (r_j^3 - 1.5 r_{s_{ij}}^3)^{1/3}. \end{aligned} \tag{A.6}$$

In the present study, terminal velocities are taken from Best (1950) and collision efficiencies from Berry (1967); the probability of coalescence $P_{CC}(i, j)$ takes into account the occurrence of multiple coalescence for the i-drop and is computed from the probability of coalescence between two colliding drops given by Brazier-Smith et al. (1972) by considering that coalescences are independent events.

The formulation of spontaneous break-up requires two probabilities. The probability for a j-drop to break up in a unit time is given by Komabayasi et al. (1964):

$$P(j) = 2.94 \cdot 10^{-7} \exp(34 r_j). \tag{A.7}$$

Taking account of the conservation of liquid water during spontaneous break-up, Srivastava (1971) has deduced the following expression for the probability $Q(i, j)$ that a fragment of the broken drop has the radius r_i:

$$Q(i, j) = \frac{62.3 \times 7}{r_i} \exp\left(-7\frac{r_j}{r_i}\right). \tag{A.8}$$

The variation of concentration of drops due to their sedimentation is represented by the vertical gradient of the flux of raindrops, so that:

$$\left(\frac{\partial n_i}{\partial t}\right)_{SED} = \frac{\partial n_i V_i}{\partial z}.$$

8.2. MPM case

The following equations are taken from Kessler (1969), but they are adapted to the unit system used in the present study.

The rate of evaporation of rain water is given by:

$$\left(\frac{\partial q_r}{\partial t}\right)_E = -\rho_a^{13/20}\, 1.93 \cdot 10^{-6} N_0^{7/20}(q_v - q_s) q_r^{13/20} \tag{A.9}$$

where $N_0 = 8 \cdot 10^6\ \mathrm{m}^{-4}$.

The rate of autoconversion of cloud to rain is given by:

$$\left(\frac{\partial q_r}{\partial t}\right)_{AUT} = -\left(\frac{\partial q_c}{\partial t}\right)_{AUT} = \frac{1}{\rho_a} 10^{-3}(\rho_a q_c - a), \tag{A.10}$$

and the rate of accretion of cloud water by raindrops by:

$$\begin{aligned} \left(\frac{\partial q_r}{\partial t}\right)_{ACC} &= -\left(\frac{\partial q_c}{\partial t}\right)_{ACC} \\ &= \rho_a 6.96 \cdot 10^{-4} N_0^{1/8} q_c q_r \exp(\beta z/2), \end{aligned} \tag{A.11}$$

where the threshold value a is taken as 0.5 g m^{-3} and the constant β as 10^{-4} m^{-1}.

The sedimentation of rain is expressed by:

$$\left(\frac{\partial q_r}{\partial t}\right)_{SED} = \frac{1}{\rho_a}\frac{\partial(\rho_a V_r q_r)}{\partial z},$$

where V_r is the fallspeed of the median volume diameter of the rain distribution. This fallspeed is given by:

$$V_r = \rho_a^{1/8}\, 38.3 N_0^{-1/8} q_r^{1/8} \exp(\beta z/2). \tag{A.12}$$

9. Appendix B

The scheme used to integrate over a time step the indexed terms of (3) representing variations in concentrations due to microphysical processes, is based on the use of redistribution functions defined by Kovetz and Olund (1969).

The variation of radius of droplets by condensation/evaporation is computed by integrating (A.2) over the time step dt_M. Since the new radius r_j' of a j-drop is not generally one of the radii previously defined, the redistribution of water droplets into the two adjacent categories is made with the redistribution functions defined by Kovetz and Olund (1969) to satisfy the requirements expressed in Subsection 3.4:

$$G_{CE}(i,j) = \begin{cases} (r_j'^3 - r_{i-1}^3)/(r_i^3 - r_{i-1}^3) & \text{if } r_{i-1} < r_j' \leqslant r_i \\ (r_{i+1}^3 - r_j'^3)/(r_{i+1}^3 - r_i^3) & \text{if } r_i < r_j' < r_{i+1} \\ 0 & \text{otherwise} \end{cases} \tag{B.1}$$

and the new concentration after a time step dt_M in the ith category is given by:

$$n_i^{t+dt} = \sum_{j=1}^{i} G_{CE}(i,j)\, n_j^*, \tag{B.2}$$

where n_j^* represents the concentration of j-drops after advection (step (i)).

The coalescence process is computed following a scheme similar to that of Kovetz and Olund (1969) by taking account of the possibility of multiple collections of smaller j-drops by an i-drop during the time step dt_M. Moreover, because of the large value of dt_M, all the n_i drops in the ith category are assumed to undergo collisions during this time step. Functions similar to those given by Kovetz and Olund (1969) are also used to redistribute water drops after coalescence, break-up by collision and production of satellite drops, respectively noted $G_{CC}(i,j)$, $G_{CB}(i,j,n)$ and $G_{SAT}(i,j,n)$. For each of these functions, the value of r_j' is deduced from (A.4), (A.6) and (A.5), respectively.

The contribution of the above processes to the ith category during a time step dt_M is given by:

$$\begin{aligned} n_i^{t+dt} &= \sum_{j=1}^{i} G_{CC}(i,j)\, n_j^* \sum_{n=1}^{j} P_{CC}(j,n)\, dt_M \\ &+ \sum_{j=i}^{N}\sum_{n=i}^{j} G_{CB}(i,j,n)\, n_j^*(1 - P_{CC}(j,n))\, dt_M \\ &+ 3\sum_{j=i}^{N}\sum_{n=i}^{j} G_{SAT}(i,j,n)\, n_j^*(1 - P_{CC}(j,n))\, dt_M \\ &- \sum_{j=i}^{N} NC(j,i)\, n_j^*\, dt_M. \end{aligned} \tag{B.3}$$

The distribution of water drops after spontaneous break-up is given by:

$$n_i^{t+dt} = \alpha_{ij} \sum_{j=i}^{N} n_j^* P(j) Q(i,j)\, dt_M \Delta r_i - n_i^* P(i)\, dt_M, \tag{B.4}$$

where r_i is the width of the ith size category. The term α_{ij} has been introduced to satisfy the conservation of liquid water, which is not maintained when discretizing the continuous formulation given by Srivastava (1971).

REFERENCES

Arnason, G. and Brown, P. S. 1971. Growth of cloud droplets by condensation: A problem in computational stability. *J. Atmos. Sci. 28*, 72–77.

Berry, E. X. 1967. Droplet growth by collection. *J. Atmos. Sci. 24*, 688–701.

Best, A. C. 1950. Empirical formulae for the terminal velocity of water drops falling through the atmosphere. *Quart. J. Roy. Meteor. Soc. 76*, 302–311.

Brazier-Smith, P. R., Jennings, S. G. and Latham, J. 1972. The interaction of falling water drops: coalescence. *Proc. Roy. Soc. London A326*, 393–408.

Brazier-Smith, P. R., Jennings, S. G. and Latham, J. 1973. Raindrop interactions and rainfall rate within clouds. *Quart. J. Roy. Meteor. Soc. 99*, 260–272.

Carbone, R. E. 1985. Comments on "Functional Fits to Some Observed Drop Size Distributions and Parameterizations of Rain". *J. Atmos. Sci. 42*, 1346–1348.

Carbone, R. E. and Nelson, L. D. 1978. The evolution of raindrop spectra in warm-based convective storms as observed and numerically modeled. *J. Atmos. Sci. 35*, 2302–2314.

Chong, M. 1983. The meteorological Doppler radars for the study of convective storms: application to the study of a tropical squall line. Doctorate thesis, University of Paris VI, 140 pp. (in French).

Hall, W. D. 1980. A detailed microphysical model within a two-dimensional dynamic framework: model description and preliminary results. *J. Atmos. Sci. 37*, 2486–2507.

Hauser, D. and Amayenc, P. 1986. Retrieval of cloud water and water vapour contents from Doppler radar data in a tropical squall line. *J. Atmos. Sci. 43*, 823–838.

Hauser, D., Amayenc, P. and Chong, M. 1984. Precipitation efficiency within a tropical squall line observed during "COPT 81" experiment. *Proc. 22nd Conf. Radar Meteorology*, Zurich, Amer. Meteor. Soc., 134–139.

Kessler, E. 1969. On the distribution and continuity of water substance in atmospheric circulation. *Meteor. Monogr. 32*, Amer. Meteor. Soc. (Boston), 83 pp.

Komabayasi, M., Gonda, T. and Isono, K. 1964. Lifetime of water drops before breaking and size distribution of fragment droplets. *J. Meteor. Soc. Japan 42*, 330–340.

Kovetz, A. and Olund, B. 1969. The effect of coalescence and condensation on rain formation in a cloud of finite vertical extent. *J. Atmos. Sci. 26*, 1060–1065.

List, R. and Gillespie, J. R. 1976. Evolution of raindrop spectra with collision-induced breakup. *J. Atmos. Sci. 33*, 2007–2013.

Long, P. E. and Pepper, D. W. 1981. An examination of some simple numerical schemes for calculating scalar advection. *J. Appl. Meteor. 20*, 146–156.

Marshall, J. S. and Palmer, W. McK. 1948. The distribution of raindrops with size. *J. Meteor. 5*, 165–166.

Mason, B. J. 1971. The growth of cloud droplets in cloud and fog. In *The physics of clouds*, 2nd ed. (ed. P. A. Sheppard). Oxford: Clarendon Press, 92–154.

Ochs III, H. T. 1978. Moment-conserving techniques for warm cloud microphysical computations. Part II. Model testing and results. *J. Atmos. Sci. 35*, 1959–1973.

Ochs III, H. T. and Yao, C. S. 1978. Moment-conserving techniques for warm cloud microphysical computations. Part I. Numerical techniques. *J. Atmos. Sci. 35*, 1947–1958.

Personne, P. 1983. Observation of bimodal spectra in stratocumuli and cumuli: their relation with entrainment. Doctorate thesis, University of Clermont-Ferrand II, 118 pp. (in French).

Purnell, D. K. 1976. Solution of the advective equation by upstream interpolation with a cubic spline. *Mon. Wea. Rev. 104*, 42–48.

Reinhardt, R. L. 1972. An analysis of improved numerical solutions to the stochastic collection equation for cloud droplets. Ph.D. thesis, University of Nevada.

Roux, F., Testud, J., Payen, M. and Pinty, B. 1984. West African squall line thermodynamic structure retrieved from dual-Doppler observations. *J. Atmos. Sci. 41*, 3104–3121.

Rutledge, S. A. and Hobbs, P. V. 1983. The mesoscale and microscale structure and organization of clouds and precipitation in midlatitude cyclones. VIII: A model for the "seeder-feeder" process in warm-frontal rainbands. *J. Atmos. Sci. 40*, 1185–1206.

Rutledge, S. A. and Hobbs, P. V. 1984. The mesoscale and microscale structure and organization of clouds and precipitation in midlatitude cyclones. XII: A diagnostic modeling study of precipitation development in narrow cold-frontal rainbands. *J. Atmos. Sci. 41*, 2949–2972.

Sekhon, R. S. and Srivastava, R. C. 1971. Doppler radar observations of drops size distributions in a thunderstorm. *J. Atmos. Sci. 28*, 983–994.

Srivastava, R. C. 1971. Size distribution of raindrops generated by their breakup and coalescence. *J. Atmos. Sci. 28*, 410–415.

Twomey, S. and Wojciechowski, T. A. 1969. Observations of the geographical variation of cloud nuclei. *J. Atmos. Sci. 26*, 684–688.

Willis, P. T. 1984. Functional fits to some observed drop size distributions and parameterization of rain. *J. Atmos. Sci. 41*, 1648–1661.

Ziegler, C. L. 1985. Retrieval of thermal and microphysical variables in observed convective storms. Part I: Model development and preliminary testing. *J. Atmos. Sci. 42*, 1487–1509.